Journal of Hazardous Materials xxx (xxxx) xxx

Contents lists available at ScienceDirect

Journal of Hazardous Materials

journal homepage: www.elsevier.com/locate/jhazmat

# UV-aging of microplastics increases proximal ARG donor-recipient adsorption and leaching of chemicals that synergistically enhance antibiotic resistance propagation

Qingbin Yuan [a], Ruonan Sun [b], Pingfeng Yu [b,c,*], Yuan Cheng [a], Wenbin Wu [a], Jiming Bao [d], Pedro J.J. Alvarez [b,**]

[a] College of Environment Science and Engineering, Nanjing Tech University, Nanjing, China
[b] Department of Civil and Environmental Engineering, Rice University, Houston, USA
[c] College of Environmental and Resource Sciences, Zhejiang University, Hangzhou, China
[d] Department of Electrical and Computer Engineering, University of Houston, Houston, USA

ARTICLE INFO

Editor: Dr. G. Jianhua

*Keywords:*
Microplastics aging
Horizontal gene transfer
Antibiotic resistance genes
Proximal adsorption
Oxidative stress
Cell permeability

ABSTRACT

Despite growing attention to environmental pollution by microplastics (MP), the effects of MP aging on bacterial horizontal gene transfer (HGT) have not been systematically investigated. Here, we used UV-aged polystyrene microplastics (PS-MPs) to investigate how aging affects antibiotic resistance genes (ARGs) transfer efficiency from various ARG vectors to recipient bacteria. The adsorption capacity of $MP_{20}$ (20-day UV-aged PS-MPs) towards *E. coli* (harboring plasmid-borne $bla_{TEM-1}$), plasmid pET29 (harboring $bla_{NDM-1}$) and phage lambda (carrying the *aphA1* ARG) increased by 6.6-, 5.2- and 8.3-fold, respectively, relative to pristine PS-MPs ($MP_0$), due to increased specific surface area and affinity for these ARG vectors. Moreover, $MP_{20}$ released more organic compounds (TOC 1.6 mg/g-$MP_{20}$, versus 0.2 mg/g-$MP_0$ in 4 h) –possibly depolymerization byproducts (verified by GC-MS), which induced intracellular ROS generation, increased cell permeability and upregulated HGT associated genes. Accordingly, $MP_{20}$ enhanced ARG transfer frequency from *E. coli*, plasmid pET29 and phage lambda (relative to $MP_0$) by 1.3-, 4.7- and 3.5-fold, respectively. The Bliss independence model infers that higher bacterial adsorption and exposure to chemicals released during MP aging synergistically enhanced ARG transfer. This underscores the need to assess the significance of this overlooked phenomenon to the environmental dissemination of antibiotic resistance and other HGT processes.

## 1. Introduction

Microplastics (MPs, defined as plastic particles within the range of 100 nm to 5 mm (Andrady, 2011)) are frequently detected in various ecosystems due to large production and improper disposal of plastics (Rochman, 2018). MPs can act as sinks and vectors of common chemical contaminants (e.g., antibiotics and heavy metals) (Fred-Ahmadu et al., 2020; Selvam et al., 2021) and microbes (e.g., algae and bacteria) (Mammo et al., 2020), which confounds their environmental impact. Antibiotic resistance genes (ARGs) are also widely distributed in natural and engineered systems (Chen et al., 2019; Karkman et al., 2019; Yuan et al., 2019), and may propagate to pathogenic bacteria through horizontal gene transfer (i.e., conjugation, transformation or transduction), which represents a threat to public health (He et al., 2020; Sun et al., 2019a; von Wintersdorff et al., 2016). Given the high probability of MP and ARG co-existence, there is a critical need to understand their interactions and implications related to environmental dissemination of antibiotic resistance.

Several studies have addressed the effects of MPs on ARG persistence and dissemination. For example, microcosm studies showed that MPs in soils or animal gut may accumulate and increase the persistence of antibiotics (Fan et al., 2021; Zhang et al., 2018), promoting resistance development. Recent quantitative PCR (qPCR) and metagenomic studies showed that ARGs were enriched in the microbial communities attached to MPs in maricultural (Zhang et al., 2020b) and activated sludge systems (Pham et al., 2021), suggesting that MPs facilitated bacterial

* Correspondence to: College of Environmental and Resource Sciences, Zhejiang University, 310058 Hangzhou, China.
** Corresponding author.
*E-mail addresses:* yupf@zju.edu.cn (P. Yu), alvarez@rice.edu (P.J.J. Alvarez).

https://doi.org/10.1016/j.jhazmat.2021.127895
Received 10 August 2021; Received in revised form 6 November 2021; Accepted 22 November 2021
Available online 25 November 2021

interactions and ARG propagation. ARGs can exist in various forms, such as intracellular plasmid-borne ARGs (iARGs), extracellular free ARGs (eARGs) and phage-borne ARGs (pARGs), which can be transferred through different potential horizontal gene transfer (HGT) mechanisms (i.e., conjugation, transformation or transduction (Ochman et al., 2000; Zarei-Baygi and Smith, 2021)). However, the effect of MPs on such processes has not been clarified, and a clear etiology on how MP aging affects ARG dissemination has not been established. This is an important knowledge gap since most related studies mainly considered pristine MPs, even though aged MPs exhibit different physicochemical properties due to fragmentation and surface oxidation as a result of mechanical abrasion, solar radiation, and biodegradation (Huffer et al., 2018; Liu et al., 2019b; Song et al., 2017). Furthermore, MPs are likely to release plastic additives and other compounds during aging because of increases in specific surface area and possible depolymerization (Lee et al., 2020; Miao et al., 2021; Tian et al., 2019), which underscores the need to investigate how these leachates influence ARG transfer mechanisms.

This study addresses how MP aging affects the transfer of different forms of ARGs (i.e., iARGs, eARGs and pARGs). Polystyrene microplastics (PS-MPs) were used as representative MPs because of their large-scale production and frequent accidental and incidental release (Liu et al., 2019b). PS-MPs were irradiated by ultraviolet radiation to accelerate aging and discern its implications on ARG transfer efficiency and mechanisms. The importance of ARG vector adsorption onto PS-MPs to enhance HGT, and of aging-related leaching on recipient bacterial susceptibility to ARG transfer, were decoupled by separately assessing HGT frequency in the presence of rinsed MPs or released leachate. Changes in affinity between PS-MPs and ARG vectors as a result of aging were examined by atomic force microscopy. The effects of MP leachate on bacterial permeability and gene expression were also considered to gain insights into accelerated HGT mechanisms. Adsorption and leachate-related processes were also considered in combination to assess potential synergism for ARG propagation. ARG transfer experiments were also conducted in activated sludge, a common urban sink of microplastics (Sun et al., 2019b), in the presence and absence of aged PS-MPs at representative concentrations.

## 2. Materials and methods

### 2.1. Preparation and characterization of PS-MPs

Whereas studies with natural MPs generally convey environmental significance, advancing mechanistic understanding of their potential environmental impacts often requires a reductionist experimental approach. Here, we used pristine MPs and investigated how artificially-accelerated aging affects their ability to promote ARG transfer through various mechanisms. About 10 g raw additive-free PS resin (Dongguan Zhongzheng Plastic, China) was mechanically ground by a grinder (FSJ-A05N6, Bear, China) for 10 min (with 0.5 min working and 0.5 min idle to avoid PS overheating). The plastic debris was then sieved sequentially via 250- and 150-μm cell strainers (Fisher Scientific, China) to obtain PS-MPs at 225.7 ± 5.3 μm. To age PS-MPs, the pristine PS-MPs ($MP_0$) were placed into quartz glass petri dishes and then irradiated under a 120 W ultraviolet-C light (254 nm, 0.34 mw/cm$^2$, Philips, Germany) for 5 and 20 days ($MP_5$ and $MP_{20}$, respectively). A 254 nm wavelength was used to accelerate the aging process, which results in similar chemical transformations exerted by longer wavelengths (Hebner and Maurer-Jones, 2020; Lin et al., 2020; Liu et al., 2019a). For reference, solar irradiation reaching earths' surface is 1.95–9.80 W/m$^2$ for UVA (300–360 nm), 0.09–0.64 W/m$^2$ for UVB (254–300 nm), and 0.02–0.08 W/m$^2$ for UVC (≤ 254 nm) (Song et al., 2017). During the irradiation, PS-MPs were blended hourly to ensure uniform exposure and the temperature was maintained at 30 °C by ventilation.

$MP_0$, $MP_5$ and $MP_{20}$ were characterized to ensure that the UV-aging process resulted in similar changes as reported for natural aging processes. Morphology was observed with a scanning electron microscopy (SEM) (Hitachi SU7000, Japan). Surface areas and pore size distributions were determined by Brunauer-Emmett-Teller (BET) surface analyzer (Autosorb-3B, Quantachrome Instruments, USA) (Biener et al., 2011). Particle size and zeta potential were measured by a Zetasizer (MS2000, Malvern Instruments, UK). Hydrophobicity was measured by an OCA-20 contact angle system (KRUSS GmbH, Germany). Functional groups were characterized by Fourier transform infrared (FTIR) spectroscopy (Nicolet iS50, Thermo-Fisher Scientific, USA) (Michielssen et al., 2020). Surface chemistry was analyzed by X-ray photoelectron spectroscopy (XPS) (250XI, Thermo-Fisher Scientific, USA) (Biener et al., 2011).

### 2.2. Preparation and characterization of PS-MP leachate

To obtain leachate (denominated $L_0$ from $MP_0$, $L_5$ from $MP_5$, and $L_{20}$ from $MP_{20}$), 300 mg PS-MPs were soaked in 3 mL distilled water and shaken (150 rpm, room temperature) for five days. The leachate was separated by centrifugation (8000 g, 10 min) and filtration by a 0.22-μm membrane. Total organic carbon (TOC) of the leachate was measured by TOC-L CPH (Shimadzu Cooperation, Japan) as previously described (González-Pleiter et al., 2019). Following accelerated UV-aging, most of the leached TOC (75–88%) was released within four hours (Fig. S1). Leachate was then collected after 4-h rinsing for subsequent experiments and characterized by excitation-emission-matrix (EEM) fluorescence spectroscopy, FTIR, and gas chromatography mass spectrometry (GC-MS, Agilent 7890A-5975 C, USA) (Capolupo et al., 2020; Chen et al., 2019; Larrieu et al., 2005).

### 2.3. Effects of PS-MPs and leachate on horizontal ARG transfer

The ARG vectors used in this study included conjugative plasmid RP4–8 harboring $bla_{TEM-1}$ (Fig. S2A) and hosted by *E. coli* BL-21, plasmid pET29(+) containing $bla_{NDM-1}$ (Fig. S2B), and lambda phage harboring the aminoglycoside resistance gene *aph*A1. *E. coli* MG1655 (labeled with chloramphenicol resistance) was selected as the recipient strain for bacteria- and phage-mediated ARG transfer, while competent strain *E. coli* DH5α (Tiangen Biotech, China) was used as host for transformation by plasmid pET29(+). ARG vectors ($10^8$ copies/mL for iARGs, $10^{10}$ copies/mL for eARGs, $10^9$ copies/mL for pARGs) and recipient bacteria ($10^8$ CFU/mL) were tested at concentrations within the range of those reported for aquatic environments and municipal wastewater treatment plants (Foladori et al., 2010; Weinbauer et al., 2004; Yuan et al., 2019). Details of ARG donor construction and HGT tests are available in the Supporting information (SI, Text S1 and S2). Briefly, non-rinsed PS-MPs (100 mg/L, with leachate), rinsed PS-MPs (100 mg/L, without leachate) or equivalent amount of leachates collected after 4-h rinsing (i.e., 14.3 μg-TOC/L for $L_0$; 83.7 μg-TOC/L for $L_5$; and 96.8 μg-TOC/L for $L_{20}$) were added to assess their effects on ARG transfer frequency. A 4-h exposure, which is sufficient to quantify HGT (Guo et al., 2015), was used for the HGT tests in the presence of MPs. This contact time ensured significant adsorption of ARG vectors onto MPs (Fig. S5) as well as a relatively constant concentration of recipient bacteria that could otherwise grow or decay significantly with longer exposure times. Note also that 4 h is within the typical range of hydraulic retention times of many wastewater treatment processes such as activated sludge (Metcalf and Eddy, 2014). The total potential recipient numbers were determined by counting colonies on LB agar plates supplemented with chloramphenicol, while the numbers of transconjugants, transformants and transductants were determined by counting colonies on LB agar with both chloramphenicol and appropriate antibiotic corresponding to the transferred ARG (i.e., ampicillin for conjugation and transformation tests, and kanamycin for transduction test). All tests were conducted in triplicate, and the corresponding ARG transfer frequency was expressed as the ratio of numbers of transconjugants, transformants and transductants to the number of recipient cells.

The interactive effects of proximal adsorption and leaching on ARG horizontal transfer were assessed using the Bliss independence model (BLISS, 1939). This involved calculation of combination indices (CI) as follows:

$$CI = (E_p + E_c - E_p \times E_c) / E_{p+c} \quad (1)$$

where $E_p$, $E_c$ and $E_{p+c}$ represents the normalized ARG transfer frequency exposed by rinsed PS-MPs, leachates, and non-rinsed PS-MPs, respectively.

### 2.4. Assessment of MP-ARG vector interfacial interactions via atomic force microscopy

Force distance (F-D) measurements were conducted on an atomic force microscopy (AFM, Park NX20, Parksystems, USA) to assess the interfacial force between various ARG vectors and non-rinsed PS-MPs of different UV-aging extents. First, the AFM tip was functionalized with bacteria, plasmids, and phages, respectively, as previously reported (Basnar et al., 2006; Doktycz et al., 2003; Fahs and Louarn, 2013; Xue et al., 2014). Specifically, *E. coli* were bound to AFM tipless cantilever via poly-L-lysine (Fig. S3A) (Doktycz et al., 2003). Thiol labeled $bla_{\text{NDM-1}}$ PCR product was bound to AFM Au-coated cantilever referring to protein through stable Au-thiol interaction (Fig. S3B). Lambda phages were bound to AFM Au-coated cantilever using crosslinkers (Fig. S3C) (Basnar et al., 2006; Fahs and Louarn, 2013; Xue et al., 2014). PS-MPs were deposited on glass slides to form homogeneous films after dissolving (Larrieu et al., 2005). Typical F-D curves with binding force and rupture forces were generated (Fig. S3D) and the most probable rupture force was obtained (Basnar et al., 2006). The details of AFM tip modification, verification, and measurement are available in the SI (Text S3 and S4 and Fig. S4).

### 2.5. Adsorption of ARG vectors by PS-MPs

Adsorption experiments were carried out to examine the affinity of PS-MPs to the ARG vectors. For adsorption kinetics measurement, 20 mg non-rinsed PS-MPs were spiked in 200 mL of phosphate buffered saline (PBS) containing separately the ARG donors (i.e., ~$10^6$ CFU/mL bacteria, ~$10^9$ copies/mL plasmids, or ~$10^7$ PFU/mL phages). The suspensions were then stirred (150 rpm) at 25 ℃ for various intervals (0.5, 2, 4, 6, 18 h, 24 h and 48 h) to characterize how adsorption of ARGs donors onto MPs reached equilibrium. To quantify the amount adsorbed, PS-MPs were collected by a cell strainer (20 μm) for DNA extraction and ARG donor quantification by qPCR. For adsorption capacity characterization, 20 mg non-rinsed PS-MPs were added to 200 mL PBS containing a series of 10-fold diluted ARG donors and then stirred (150 rpm) at 25 ℃ for 18 h, which was sufficient to reach equilibrium (Fig. S5). PS-MPs were then collected by a cell strainer (20 μm) for ARG donor quantification. Details about qPCRs analyses in terms of primer sets, reaction reagents, and running programs are available in the SI (Text S5 and Table S1). ARG vector adsorption capacity and rates were determined by fitting adsorption isotherm data to a first-order kinetic and the Langmuir isotherm model, respectively (Vieira et al., 2018).

The adsorbed iARG, eARG, and pARG on MPs were stained with DAPI (Beyotime Biotechnology, China), Gel-green (Beyotime Biotechnology, China), and SYTO-9 (Thermo Fisher Scientific, USA), respectively. Briefly, non-rinsed PS-MPs after iARG, eARG, and pARG adsorption for 60 min were fixed with glutaraldehyde (v/v, 2.5%) overnight. The PS-MPs were rinsed twice with PBS and then incubated in the corresponding dye solution for 15 min. Stained samples were washed twice with PBS, dried in a desiccator, and observed under the fluorescence microscope. The excitation and emission wavelength (Ex/Em) were 340/488 nm for iARG, 497/540 nm for eARG, and 485/498 nm for pARG, respectively.

### 2.6. Effects of PS-MPs and leachate on recipient bacterial cells

The effects of non-rinsed PS-MPs, rinsed PS-MPs, and the leachates on the permeability of potential ARG recipient cells (*E. coli* MG1655) were examined since this is a key factor in ARG horizontal transfer (Han et al., 2020; Jin et al., 2020; Zhang et al., 2021a). Cell permeability was evaluated by lactate dehydrogenase (LDH) assay (Liu et al., 2013). Briefly, ARG recipients (~$10^7$ CFU/mL) were exposed to (A) 100 mg non-rinsed or rinsed PS-MPs/L, (B) 1 mL/L leachate (i.e., 14.3 μg-TOC/L for $L_0$; 83.7 μg-TOC/L for $L_5$; and 96.8 μg-TOC/L for $L_{20}$) collected by 4-h rinsing by stirring in PBS (300 rpm), and (C) PBS buffer as control group. Cells were then collected separately and transferred into 96-well plates to mix with 50 μL substrate mixture (Roche Applied Science, Switzerland). After 30 min incubation at room temperature (25 °C) in the dark, 50 μL stop solution (Roche Applied Science, Switzerland) was added to each well and the absorbance at 490 nm was recorded using the Plate Reader (Infinite M Plex, TECAN, Switzerland).

Intracellular reactive oxygen species (ROS) production, which can affect cell permeability (Jin et al., 2020), was also assessed. The response of intracellular ROS to non-rinsed PS-MPs, rinsed PS-MPs and the leachates was measured by the Dichlorofluorescein Fluorescence Kit (KeyGEN BioTECH, China) (Liu et al., 2013). The recipient cells were exposed to 100 mg/L PS-MPs (or equivalent leachate) for four hours. Thereafter, the recipient cells were washed by PBS for three times, spiked with 2′,7′-dichlorodihydrofluorescein diacetate ($H_2$DCFDA) solution with a final concentration of 10 μM, and then incubated for 30 min in darkness. After incubation, cells were washed by PBS for three times, and the fluorescence was measured on the plate reader with the excitation and emission wavelength at 495 nm and 525 nm, respectively. Cells without PS-MPs or leachate treatment were also measured as negative controls. To further verify the effect of ROS on cell permeability, a ROS scavenger, N-acetyl-L-cysteine (final amount = 100 μM), was added and the production of LDH and ROS was monitored.

### 2.7. Differential gene expression analysis

Following 4-h exposure to non-rinsed PS-MPs (100 mg/L) or leachate (1 mL/L), donor bacteria *E. coli* BL-21 were sampled for transcriptomic analysis of two genes regulating conjugation (i.e., *kilA* and *traI*) (Wang et al., 2015). For phage sensitivity assessment, recipient bacteria *E. coli* MG1655 were collected for transcriptomic analysis of two genes regulating bacterial sensitivity to phage lambda (i.e., *lamB* encoding the receptor of phage lambda (Emr et al., 1978) and *malT* encoding the positive regulator of *lamB* (Marchal et al., 1980)). Transcriptomic analysis of genes associated with intracellular ROS production (i.e., SOS repressor gene *lexA* and SOS response gene *recA* (Yang et al., 2019)) and bacterial cell permeability (i.e., gene *ompR*) of recipient bacteria *E. coli* MG1655 (Yu et al., 2021) was also conducted. The 16S rRNA gene, which exhibits relatively stable expression in bacteria, was used as the reference gene for gene expression normalization (Huang et al., 2014). Bacterial samples were subjected to RNA extraction, purification, and quantification using the RNAprep pure Cell Kit (Tiangen Biotech, China) following the manufacturer's instructions. Subsequently, reverse transcription-polymerase chain reaction (RT-PCR) analysis was conducted to obtain the cDNA with FastKing RT Kit (Tiangen Biotech, China). Triplicate qPCR reactions were conducted to identify the cycle threshold (CT) values for the target and reference genes, and the $2^{-\Delta\Delta CT}$ method was used to quantify differential gene expression relative to the reference gene (Zhang et al., 2020a). Detailed information about primers is listed in Table S2.

### 2.8. Effects of PS-MPs on ARG propagation in activated sludge

Municipal wastewater treatment plants are common sinks for MPs, where they reach concentrations up to 7000 particles per kg wet weight (Sun et al., 2019b). Here, non-rinsed PS-MPs (100 mg/L, equaling about

10,000 particles/L) were spiked into microcosms containing 200 mL activated sludge (with characteristics presented in Table S3) collected from a local municipal wastewater treatment plant (WWTP, Nanjing, China). These microcosms were shaken with 150 rpm at 25 °C. After 4-h treatment, the PS-MPs were removed via a cell strainer (20 μm) and the microbial samples were processed for intracellular DNA extraction. Specifically, the biomass was retained on a 0.22-μm membrane and then subject to intracellular DNA extraction using Fast DNA™ SPIN kit for soil (MP Biomedicals, USA). Two widely reported ARGs in wastewater (i.e., *tetA* and *sulI*) (Wang et al. (2021); Pazda (2019)) and 16 S rDNA gene were then quantified by qPCR to assess the relative abundance of each ARG.

### 2.9. Statistical analysis

The ANOVA and Student *t*-test with Bonferonni correction for multiple comparisons conducted by SPSS software (IBM SPSS Statistics, USA) were used to determine statistical significance at $p = 0.05$ level. Based on the Bliss independence model, the combined effect of proximal adsorption and leachate was considered synergistic when $CI < 1$ or antagonistic when $CI > 1$ (BLISS, 1939).

## 3. Results and discussion

### 3.1. UV irradiation increased PS-MP surface area and oxidation state

Similar to the natural aging process (Brandon et al., 2016; Song et al., 2017), UV irradiation substantially altered the surface chemistry and morphology of PS-MPs. Whereas $MP_0$ exhibited intact and smooth surface, $MP_5$ had racks and wrinkles on its surface and $MP_{20}$ had nanosheets and nanopores on its surface (Fig. S6), probably due to MP embrittlement and fracturing (Liu et al., 2019b). Accordingly, there were consistent increases in total pore volumes and specific surface areas along the simulated aging process (Fig. 1A&1B). Additionally, the average particle size decreased from 225.7.0 ± 5.3–207.9 ± 2.3 μm for $MP_5$ and 201.9 ± 3.4 μm for $MP_{20}$ after aging, and the specific surface area increased from 0.82 $m^2/g$ to 1.34 $m^2/g$ for $MP_5$ and 1.67 $m^2/g$ for $MP_{20}$ (Table S4).

The FTIR spectrum showed an increase in oxygen-containing functional groups after UV irradiation (Fig. 1C). Absorption peaks at 1720 $cm^{-1}$ and 2800–3200 $cm^{-1}$, which respectively correspond to C═O-OH and -OH vibration stretches, were significantly amplified after aging. The XPS spectrum corroborated that oxygen-containing functional groups (i.e., 286.2 eV for C-O-C and 288.4 eV for C═O-OH) appeared after aging while the characteristic functional groups of pristine PS (i.e., 284.6 eV for aromatic C-H and 291.2 eV for π-π stacking) decreased dramatically (Fig. 1D). Accordingly, the hydrophobicity of the aged PS was substantially lower than that of the pristine PS with water contact angles 101.0° for $MP_0$, 93.3° for $MP_5$ and 92.4° for $MP_{20}$ (Table S4). These changes after short-time UV irradiation were consistent with those reported after long-term weathering in natural environments (Brandon et al., 2016; Song et al., 2017). Therefore, these PS-MPs (i.e., $MP_0$, $MP_5$ and $MP_{20}$) were used to investigate how MP aging affects horizontal ARG transfer.

### 3.2. UV-aged PS-MPs enhanced horizontal ARG transfer compared to pristine PS-MPs

Non-rinsed MPs increased HGT frequency in PBS medium relative to the control groups without MPs for all three vectors (Fig. 2 A-C).

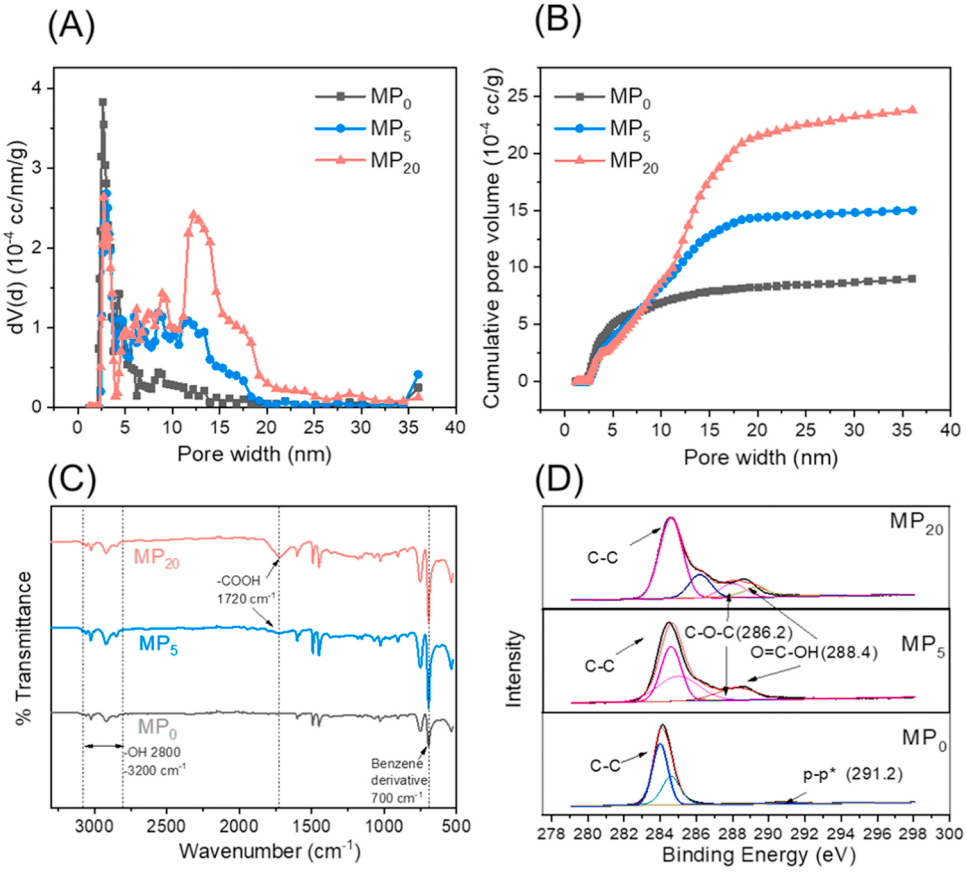


**Fig. 1.** Physical and chemical changes of PS-MPs due to UV irradiation. The pristine PS-MPs ($MP_0$) were irradiated under UVC (254 nm, 0.34 mw/$cm^2$) for 5 and 20 days to obtain 5-day aged and 20-day aged PS-MPs ($MP_5$ and $MP_{20}$), respectively. Panels A and B show the nanopore size distribution and cumulative pore volume of $MP_0$, $MP_5$, and $MP_{20}$, respectively. Panels C and D show surface chemistry changes by FTIR and XPS of $MP_0$, $MP_5$, and $MP_{20}$, respectively.

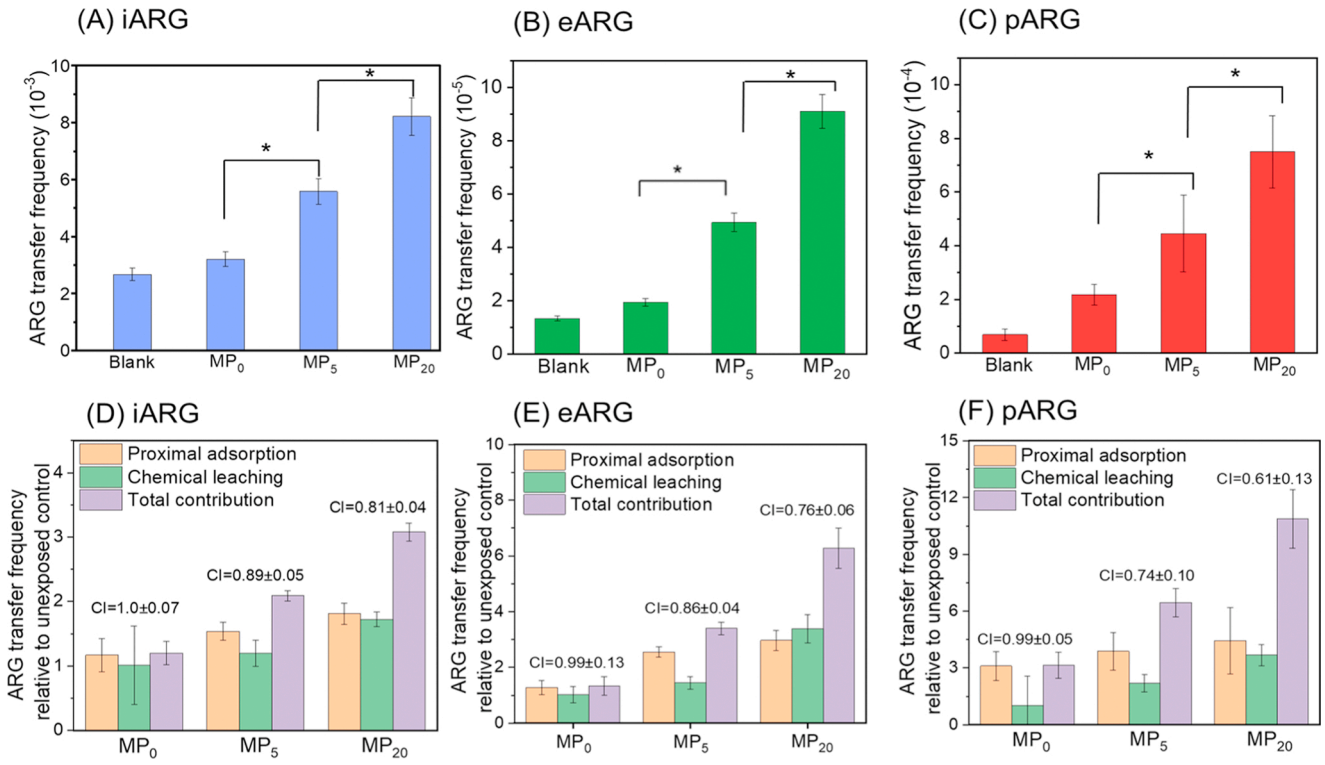


**Fig. 2.** PS-MP aging enhanced various horizontal gene transfer mechanisms in PBS medium. Non-rinsed MPs increased the transfer frequencies of iARGs (A), eARGs (B), and pARGs (C) in PBS medium, with more aged MPs resulting in more significant stimulation. Asterisks (*) represent significant differences ($p < 0.05$) based on Student's *t*-test. The transfer frequencies of iARGs (D), eARGs (E), or pARGs (F) were quantified after exposure to rinsed PS-MPs (proximal adsorption), leachate (chemical leaching), or non-rinsed PS-MPs (total contribution) relative to unexposed control. The concentrations of PS-MPs were 100 mg/L, and the leachate TOC concentrations were 14.3 μg-/L for $MP_0$, 83.7 μg-/L for $MP_5$, and 96.8 μg/L for $MP_{20}$. Error bars in all the figures represent ± one standard deviation from the mean of independent triplicates.

Specifically, the transfer frequency of iARGs, eARGs, and pARGs in the presence of $MP_0$ were $3.2 \times 10^{-3}$, $1.9 \times 10^{-5}$, and $2.2 \times 10^{-4}$, which represents 1.2-, 1.5-, and 3.1-fold increases relative to the unexposed control groups. Aged PS-MPs (i.e., $MP_5$ and $MP_{20}$) further increased the gene transfer frequency. Relative to the control groups, the transfer frequency of iARGs, eARGs, and pARGs in the presence of $MP_5$ increased by 1.3-, 3.7-, and 6.5-fold, respectively. $MP_{20}$ further increased the corresponding gene transfer frequency by 1.6-, 6.8-, and 10.9-fold.

Conjugation is generally the dominant mechanism of ARG horizontal dissemination, due to the high transfer frequency and abundance of intracellular plasmid-borne ARGs (Dang et al., 2017). Transduction can also be an important ARG transfer mechanism, since numerous studies showed that phages are significant ARG vectors in various environments (Calero-Cáceres et al., 2014, 2017; Calero-Caceres and Muniesa, 2016; Yang et al., 2018). Transformation could also contribute to HGT, but this requires eARGs and competent bacteria to co-exist with high abundance (Dong et al., 2019; Yuan et al., 2020). In this work, consistent with the literature (Jiang et al., 2017), transformation was a relatively minor HGT mechanism compared to conjugation and transduction (Fig. 2), despite the highly favorable conditions used (i.e., proximity of eARGs and competent bacteria at relatively high concentrations). The enhanced HGT by aged MPs (in the absence of antibiotics) underscores the overlooked risk of antibiotic resistance development in many environments where MPs and ARGs frequently cooccur and the risk can be significantly enhanced by gradually aged MPs.

For pristine non-rinsed PS-MPs, HGT enhancement was mainly caused by proximal adsorption of ARG donors and recipients, while the contribution from the leachates was marginal (Fig. 2 D-F). For aged non-rinsed PS-MPs, both adsorption and leachate contributed to the enhanced ARG transfer frequency, and the latter became more predominant with increased aging (Fig. 2 D-F). For example, the leachate from $MP_{20}$ increased HGT frequency by 1.7–3.7-fold while rinsed $MP_{20}$ increased HGT frequency by 1.8–4.4-fold (Fig. 2 D-F). Apparently, stress exerted by leachate from aging MPs stimulated HGT as reported for sublethal stress from antibiotics and heavy metals (Andersson et al., 2014; Gullberg et al., 2014).

### 3.3. *UV-aged PS-MPs exhibited higher adsorption affinity for both ARG donors and recipients*

The interactive force between ARG donors and non-rinsed PS-MPs was positively correlated with the extent of MP aging. The most probable rupture force between ARB and PS-MPs increased from 77.5 ± 1.8 nN for $MP_0$ to 121.2 ± 0.2 nN for $MP_5$, and further increased to 147.6 ± 0.7 nN for $MP_{20}$ (Fig. S7 A-C). Similar trends were observed for the force between eDNA and PS-MPs (Fig. S7 D-F) and that between phages and PS-MPs (Fig. S7 G-I). Whereas pristine MPs mainly interact with biological components via hydrophobic attraction and π-π stacking (Jucker et al., 1998), the aged PS-MPs with more oxygen-containing functional groups (e.g., C═O-OH) on the surface may form more stable hydrogen bonds with the ARG vectors (Mei et al., 2020). Moreover, the nanopore and nanosheet structure on the aged PS-MPs surface may also contribute to the stronger interactive force due to improved contact surface (De et al., 2008).

A stronger interactive force contributed to the enhanced adsorption capacity of non-rinsed PS-MPs towards both ARG donors and recipients (Fig. 3 A-C). Whereas adsorption of ARG donors by the tested MPs generally followed first-order kinetics (Table S5), the MPs exhibited faster adsorption with rate constants with $MP_{20}$ for bacteria, eDNA, and phages 2.8-, 2.3-, and 1.9-times higher than those with $MP_0$, respectively. Furthermore, the adsorption isotherms of bacteria and phages were adequately fit by the Langmuir isotherm model (Table S6),

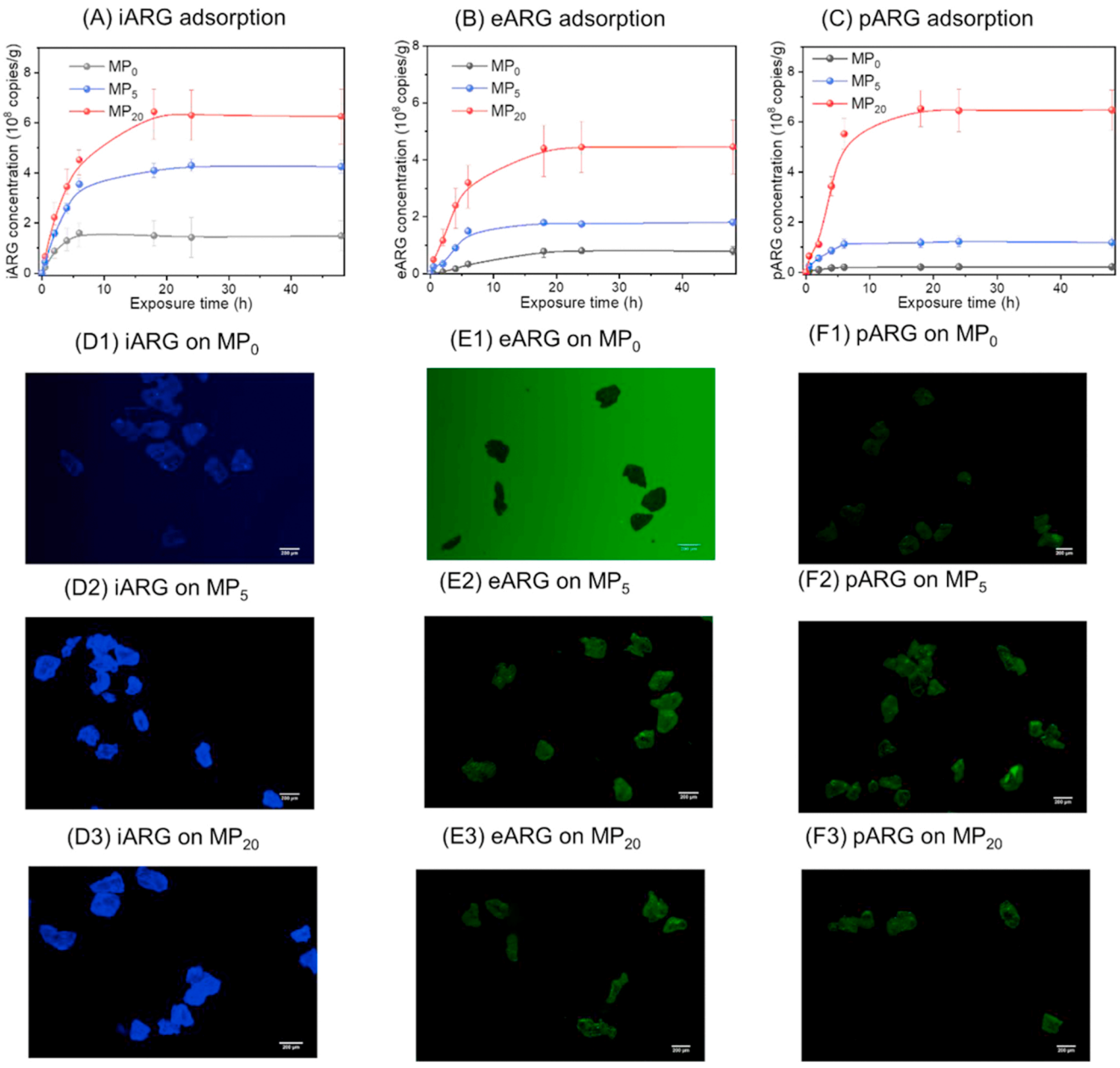


**Fig. 3.** Adsorption of ARG donors on different aged MPs without rinsing (100 mg/L) in PBS. Adsorption kinetics increased with MP aging for bacteria (A), eDNA (B), and phages (C). The initial free ARG donor levels were ~$10^6$ CFU/mL bacteria, ~$10^9$ copies/mL plasmids, and ~$10^7$ PFU/mL phages. Fluorescent microscopic imaging of bacteria, plasmids, and phages adsorbed on $MP_0$ (D1~F1), MP5 (D2~F2), and $MP_{20}$ (D3~F3). The bacteria, eDNA, and phages were stained with DAPI, gel-green, and SYTO-9, respectively. Scale bars represent 200 μm.

suggesting monolayer adsorption of ARG donors on the MP surface (Wang and Wang, 2018). However, the adsorption capacity of $MP_{20}$ for bacteria, eDNA, and phages was 6.6-, 5.2- and 8.3-times higher than that of $MP_0$, respectively (Table S6). Enhanced adsorption of ARG vectors by aged PS-MPs was also verified by fluorescent microscopic imaging, which showed higher fluorescence intensity (emitted by the stained ARG donors) on the aged PS-MPs (Fig. 3).

UV-aging also enhanced the retention of ARG donors and recipients on PS-MPs. Both ARG donors and recipients were more difficult to desorb from aged PS-MPs than the pristine PS-MPs (Fig. S8 and S9). Specifically, 85.8%, 88.3%, and 62.5% bacteria, eDNA, and phages were desorbed from $MP_0$ in 60 min, while only 73.6%, 64.1%, and 13.3% were desorbed from $MP_{20}$. This suggests a higher chance of interactions between ARG donors and recipients on the aged MP surface, which is conducive to enhanced ARG transfer (Hermansson and Linberg, 1994).

### *3.4. UV-aged PS-MPs enhance the susceptibility of recipient bacteria to ARG transfer.*

Non-rinsed $MP_0$, $MP_5$, and $MP_{20}$ increased cell permeability relative to unexposed controls, as indicated by an increase in LDH release by 5.4-, 6.1-, and 7.9-fold, respectively (Fig. 4A). This is corroborated by increased cell surface roughness after exposure to aged MPs, based on the AFM analysis (Fig. S10). A positive (though relatively weak) correlation was observed between LDH release and ARG transfer frequency ($R^2$ = 0.70–0.93, $p$ = 0.02–0.10). Apparently, the increase in cell permeability facilitated HGT, by both enhancing release of resistance plasmids from donors (for conjugation) and facilitating ARG uptake by recipients (by conjugation or transformation) (Qiu et al., 2012; Zhang et al., 2021b).

Consistent with previous reports (Liu et al., 2018; Qiu et al., 2012),

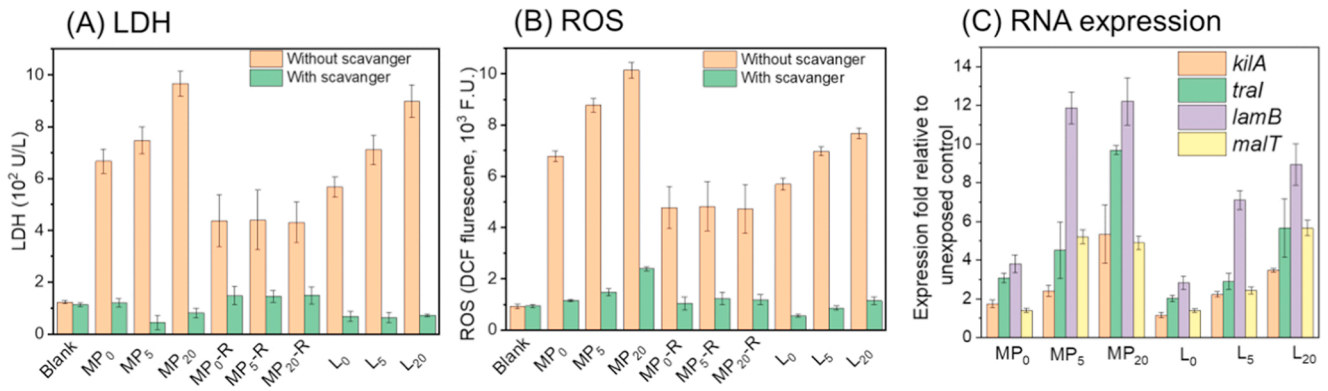


**Fig. 4.** Bacterial response to PS-MPs and leachates from different aged PS-MPs. Panels depict (A) changes in cell permeability (LDH release); (B) More pronounced intracellular ROS production when recipient bacteria were exposed to non-rinsed PS-MPs or leachate from PS-MPs aged to a greater extent; and (C) upregulation of genes associated with HGT (i.e., *kilA* and *traI* for conjugation and *lamB* and *malT* for phage infection) after exposure to non-rinsed MPs or leachates. $MP_0$, $MP_5$, and $MP_{20}$ represent non-rinsed PS-MPs aged for 0, 5, and 20 d, respectively. $L_0$, $L_5$ and $L_{20}$ represent leachates from PS-MPs aged for 0, 5, and 20 d, respectively. The concentrations of PS-MPs were 100 mg/L, and the leachate TOC concentrations were 14.3 μg /L for $L_0$, 83.7 μg/L for $L_5$, and 96.8 μg /L for $L_{20}$.

oxidative stress (e.g., intracellular ROS accumulation) – likely induced by chemicals released by aging PS-MPs — contributed to the observed increase in cell permeability (Fig. 4B). The resulting intracellular ROS accumulation increased by 7.3-, 9.4-, and 10.9-fold after exposure to non-rinsed $MP_0$, $MP_5$, and $MP_{20}$, respectively (Fig. 4B), which was positively correlated with the increase in LDH release ($R^2 = 0.82$, $p < 0.05$). In the presence of ROS scavenger (100 μM N-acetyl-L-cysteine), exposure to PS-MPs resulted in significantly less intracellular ROS accumulation and corresponding LDH release (Fig. 4A and B). Accordingly, the ARG transfer efficiency decreased significantly to a similar level as that resulting from exposure to rinsed MPs (i.e., without leached chemicals) (Fig. S11).

Transcriptomic effects of non-rinsed PS-MPs were also considered to gain insight into accelerated HGT mechanisms. Two genes regulating ARG conjugation (*kilA* and *traI*) were upregulated slightly by 1.6 ~ 3.1-fold upon exposure to $MP_0$ relative to control groups without PS-MP exposure (Fig. 4C). Aged PS-MPs upregulated both genes to a larger extent (5.3- to 9.7- fold) upon exposure to $MP_{20}$ (Fig. 4C). Aged PS-MPs also upregulated genes associated with phage infection (i.e., *lamB* and *malT*) more significantly relative to pristine PS-MPs (Fig. 4C). Upregulation of genes associated with cell permeability (e.g., *ompR*) and intracellular ROS production (e.g., SOS response gene *recA*) was also

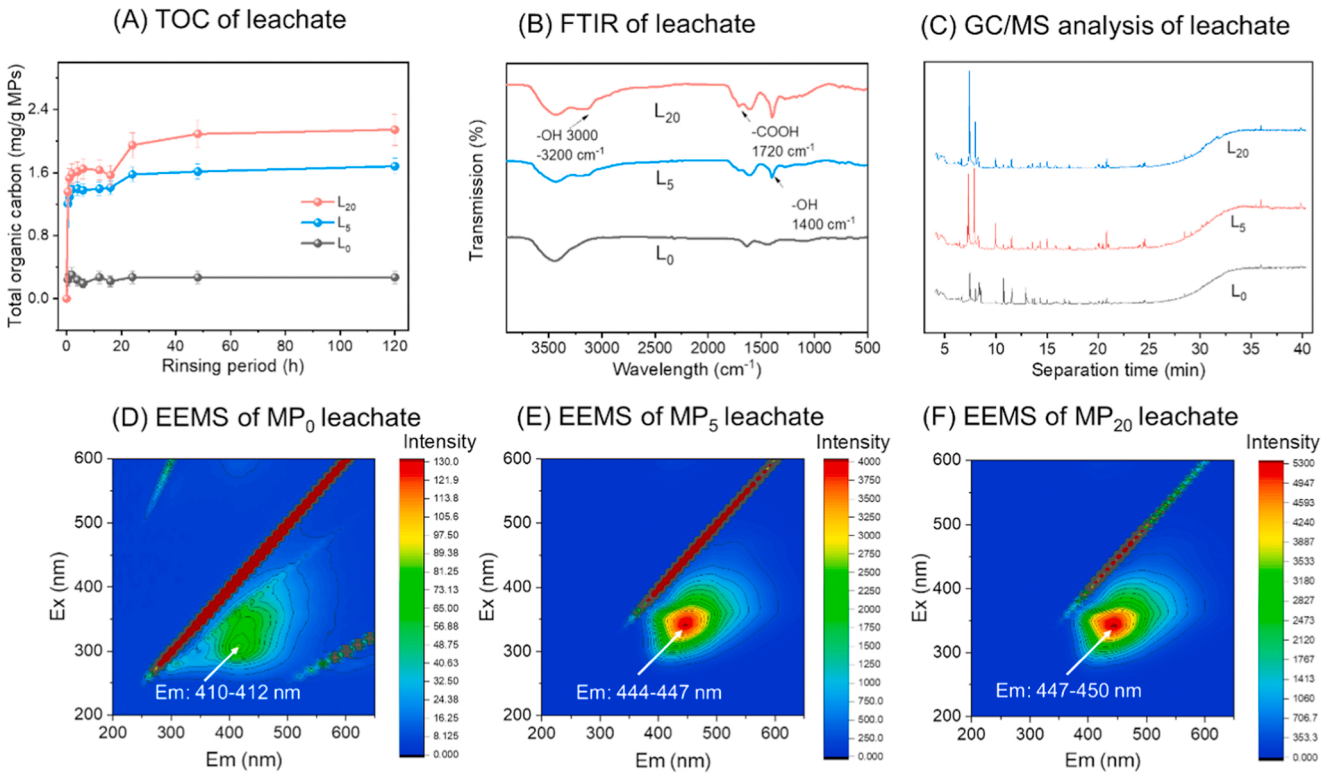


**Fig. 5.** Characterization of leachates from pristine and aged microplastics. (A) Aged MPs released more chemicals as reflected by higher total organic carbon (TOC) in the rinse solution. Leachate from more aged MPs had higher abundance of oxidized groups indicated by FTIR analysis (B) and smaller molecules as reflected by shorter GC-MS retention time (C). EEM analysis ($\lambda_{ex}/\lambda_{em}$ = 300–350/400–450 nm) of leachates from $MP_0$ (D), $MP_5$ (E), and $MP_{20}$ (F) corroborated the facilitated release of low molecular organic chemicals from aged microplastics, as indicated by increase of the florescence intensity and the red shift of the peak. $E_m$ and $E_x$ represent emission and excitation wavelengths, respectively. $L_0$, $L_5$, and $L_{20}$ represent leachates from PS-MPs aged for 0, 5, and 20 days, respectively.

observed when the recipient bacteria were exposed to UV-aged PS-MPs (Fig. S12), which was conductive to enhanced HGT.

### 3.5. The contribution of PS-MP leachate on ARG transfer increased with UV-induced aging

Whereas pristine MPs released some organic chemicals (i.e., 0.2 mg-TOC/g $MP_0$), UV aging accelerated TOC release by 4.8-fold for $MP_5$ (1.4 mg-TOC/g $MP_5$) and by 5.7-fold for $MP_{20}$ (1.6-TOC mg/g $MP_{20}$) over four-hour rinsing (Fig. 5 A). UV-induced MP aging enhanced the release of organic chemicals from MPs as a result of increased surface areas and oxidation-induced depolymerization of MPs. Specifically, $L_5$ and $L_{20}$ contained more different compounds and more oxygen functional groups than $L_0$ (Fig. 5 B and C). Moreover, a significant red shift of the peak was observed for $L_5$ and $L_{20}$ (Fig. 5D-F), suggesting an increase in released low molecular weight organics after MP aging (Lavonen et al., 2014; Chai et al., 2012).

Leachates from aged MPs induced more intracellular ROS than those from pristine MPs at the same TOC level (i.e., 0.2 mg/g MPs) (Fig. S10), indicating that fragmented and oxidized chemicals produced by UV-aging may exert higher oxidative stress on bacteria (Tian et al., 2019). Consistently, when bacteria were exposed to the more aged PS-MPs or their leachates, more intracellular ROS was produced and cell permeability increased to a greater extent (Fig. 4A&4B). Furthermore, leachates from aged PS-MPs upregulated genes associated with HGT to a greater extent than leachates from pristine PS-MPs (Fig. 4C). Overall, PS-MPs aging accelerated the release of organic compounds, increasing cell susceptibility to ARG transfer.

The *CI* values calculated by the Bliss independence model were near 1.0 for the pristine MPs but decreased significantly below 1.0 with aging (Fig. 2 D-F), which indicates a significant synergistic stimulation of HGT by the presence of aged MP surfaces and leachates. Aging not only increased MP surface area and its affinity to both ARG donors and recipients, enhancing opportunities for their proximal adsorption, but also promoted the released chemicals that increased the susceptibility of recipient cells for gene transfer. Therefore, aging significantly increased the efficiency of ARG propagation even in the absence of selective pressure by residual antibiotics.

### 3.6. UV-aged PS-MPs enhanced horizontal transfer of ARGs in activated sludge microcosms.

In the activated sludge microcosms, pristine MPs (100 mg/L) did not significantly enhance the propagation of two common ARGs (i.e., *tetA* and *sulI*) over four hours (Fig. 6). Apparently, the surface area contribution of MPs was small relative to that of the more abundant background suspended solids (MLSS = 3500 mg/L). However, the intracellular concentration of *tetA* and *sulI* significantly increased in the presence of aged MPs that released more byproducts (Fig. 6). Specifically, the relative abundance of *tetA* and *sulI* in activated sludge increased significantly ($p < 0.05$) from $(1.0 \pm 0.9)\times 10^{-2}$ and $(8.2 \pm 1.5)\times 10^{-3}$, respectively, in the absence of MPs, to $(4.5 \pm 1.2)\times 10^{-2}$ and $(1.1 \pm 0.2)\times 10^{-2}$ with $MP_5$, and further to $(6.0 \pm 1.4)\times 10^{-2}$ and $(1.3 \pm 0.2)\times 10^{-2}$ with $MP_{20}$ (i.e., 6- and 1.6-fold increases, respectively).

The release dynamics of compounds from aging MPs can be confounded by the environmental matrix and dilution potential, and their region of influence may be limited to the immediate MP surroundings. However, the aged PS-MP surface may serve as an aggregation site and accelerator of HGT by bringing susceptible bacteria into facilitated contact with each other and with released chemicals. This potentially synergistic combination of greater surface area for proximal adsorption of gene vectors (e.g., donor bacteria, transforming eDNA, and transducing phages) and recipient cells, and release of HGT-facilitating chemicals may lead to an enrichment of the environmental resistome even in the absence of antibiotics. These overlooked phenomena are important to characterize, given the critical role of HGT in microbial adaptation and dissemination of beneficial (e.g., catabolic) or problematic (e.g., pathogenic) genes.

## 4. Conclusion

Due to increased surface area and higher affinity to ARG vectors (e.g., bacteria, phages, and plasmids) and recipient cells, aged MP surfaces offer opportunities for their proximal adsorption, which is conducive to enhanced ARG transfer and other HGT processes. Furthermore, the chemicals released during MP aging under light irradiation (likely depolymerization byproducts) increased the susceptibility of recipient cell to HGT, both through membrane permeabilization and upregulation of genes associated with gene uptake. The combination of proximal adsorption and leaching processes during MP aging can synergistically enhance HGT, which may enrich the environmental resistome even in the absence of antibiotics. This underscores the need to assess the scale and significance of this overlooked phenomenon, with particular regard to implications on public health (e.g., environmental ARG or pathogenic genes dissemination) and critical microbial processes (e.g., biogeochemical cycling). Accordingly, future research is warranted to identify and scrutinize other materials that hold the potential to enhance HGT by similar mechanisms.

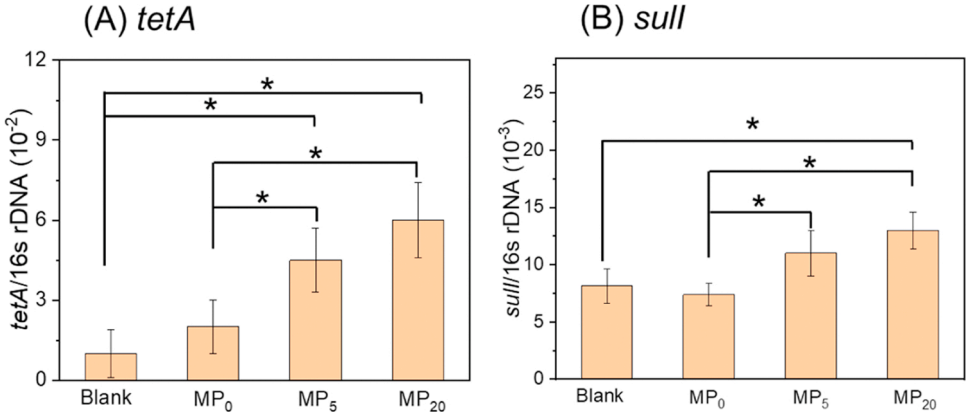


**Fig. 6.** The influence of pristine versus aged microplastics on ARG propagation in activated sludge. The relative abundance of intracellular *tetA* and *sulI* in activated sludge increased significantly after four-hour exposure to 100 mg/L non-rinsed $MP_{20}$. Asterisks (*) indicates significantly difference of ARG relative abundance between different groups.

## CRediT authorship contribution statement

Qingbin Yuan, Investigation, Methodology, Validation, Formal analysis, Writing - Original draft preparation, Funding acquisition., Ruonan Sun, Investigation, Methodology, Formal analysis, Writing - Original draft preparation, Pingfeng Yu*, Conceptualization, Investigation, Methodology, Formal analysis, Writing - Original draft preparation, Review & Editing., Yuan Cheng, Investigation, Methodology, Validation, Wenbin Wu, Investigation, Methodology, Validation., Jiming Bao, Investigation, Methodology, Resources. Pedro J. J. Alvarez*,Conceptualization, Supervision, Funding acquisition, Project administration, Writing - Review & Editing.

## Declaration of Competing Interest

The authors declare that they have no known competing financial interests or personal relationships that could have appeared to influence the work reported in this paper.

## Acknowledgments

This study was supported by Natural Science Foundation of Jiangsu Province [grant number BK20201367], National Natural Science Foundation of China [grant number 42177348], and the NSF ERC on Nanotechnology-Enabled Water Treatment (EEC-1449500). Qingbing Yuan received partial financial support from China Scholarship of Council.

*Supplementary materials*

includes AFM cantilevers functionalization methods with ARG vectors, phage lambda modification with ARGs, characterization of microplastics in terms of morphology and affinity to ARG vectors, assessment of bacterial surface after microplastic exposure, and details of ARG quantitation via qPCR.

## Appendix A. Supporting information

Supplementary data associated with this article can be found in the online version at doi:10.1016/j.jhazmat.2021.127895.

## References

Andersson, D.I., Hughes, D., 2014. Microbiological effects of sublethal levels of antibiotics. Nat. Rev. Microbiol. 12 (7), 465–478.
Andrady, A.L., 2011. Microplastics in the marine environment. Mar. Pollut. Bull. 62 (8), 1596–1605.
Basnar, B., Elnathan, R., Willner, I., 2006. Following aptamer−thrombin binding by force measurements. Anal. Chem. 78 (11), 3638–3642.
Biener, J., Stadermann, M., Suss, M., Worsley, M.A., Biener, M.M., Rose, K.A., Baumann, T.F., 2011. Advanced carbon aerogels for energy applications. Energ. Environ. Sci. 4 (3), 656–667.
BLISS, C.I., 1939. The toxicity of poisons applied jointly 1. Ann. Appl. Biol. 26 (3), 585–615.
Brandon, J., Goldstein, M., Ohman, M.D., 2016. Long-term aging and degradation of microplastic particles: comparing in situ oceanic and experimental weathering patterns. Mar. Pollut. Bull. 110 (1), 299–308.
Calero-Caceres, W., Muniesa, M., 2016. Persistence of naturally occurring antibiotic resistance genes in the bacteria and bacteriophage fractions of wastewater. Water Res. 95, 11–18.
Calero-Cáceres, W., Melgarejo, A., Colomer-Lluch, M., Stoll, C., Lucena, F., Jofre, J., Muniesa, M., 2014. Sludge as a potential important source of antibiotic resistance genes in both the bacterial and bacteriophage fractions. Environ. Sci. Technol. 48 (13), 7602–7611.
Calero-Cáceres, W., Méndez, J., Martín-Díaz, J., Muniesa, M., 2017. The occurrence of antibiotic resistance genes in a Mediterranean river and their persistence in the riverbed sediment. Environ. Pollut. 223, 384–394.
Capolupo, M., Sørensen, L., Jayasena, K.D.R., Booth, A.M., Fabbri, E., 2020. Chemical composition and ecotoxicity of plastic and car tire rubber leachates to aquatic organisms. Water Res. 169, 115270.
Chai, X., Liu, G., Zhao, X., Hao, Y., Zhao, Y., 2012. Fluorescence excitation–emission matrix combined with regional integration analysis to characterize the composition and transformation of humic and fulvic acids from landfill at different stabilization stages. Waste Manag. 32 (3), 438–447.
Chen, Y., Su, J.-Q., Zhang, J., Li, P., Chen, H., Zhang, B., Gin, K.Y.-H., He, Y., 2019. High-throughput profiling of antibiotic resistance gene dynamic in a drinking water river-reservoir system. Water Res. 149, 179–189.
Dang, B., Mao, D., Xu, Y., Luo, Y., 2017. Conjugative multi-resistant plasmids in Haihe River and their impacts on the abundance and spatial distribution of antibiotic resistance genes. Water Res. 111, 81–91.
De, M., Ghosh, P.S., Rotello, V.M., 2008. Applications of nanoparticles in biology. Adv. Mater. 20 (22), 4225–4241.
Doktycz, M.J., Sullivan, C.J., Hoyt, P.R., Pelletier, D.A., Wu, S., Allison, D.P., 2003. AFM imaging of bacteria in liquid media immobilized on gelatin coated mica surfaces. Ultramicroscopy 97 (1), 209–216.
Dong, P., Wang, H., Fang, T., Wang, Y., Ye, Q., 2019. Assessment of extracellular antibiotic resistance genes (eARGs) in typical environmental samples and the transforming ability of eARG. Environ. Int. 125, 90–96.
Emr, S.D., Schwartz, M. and Silhavy, T.J., 1978. Mutations altering the cellular localization of the phage lambda receptor, an *Escherichia coli* outer membrane protein. Proc. Natl. Acad. Sci. U. S. A. 75 (12), 5802–5806.
Fahs, A., Louarn, G., 2013. Plant protein interactions studied using AFM force spectroscopy: nanomechanical and adhesion properties. Phys. Chem. Chem. Phys. 15 (27), 11339–11348.
Fan, X., Zou, Y., Geng, N., Liu, J., Hou, J., Li, D., Yang, C., Li, Y., 2021. Investigation on the adsorption and desorption behaviors of antibiotics by degradable MPs with or without UV ageing process. J. Hazard. Mater. 401, 123363.
Foladori, P., Bruni, L., Tamburini, S., Ziglio, G., 2010. Direct quantification of bacterial biomass in influent, effluent and activated sludge of wastewater treatment plants by using flow cytometry. Water Res. 44 (13), 3807–3818.
Fred-Ahmadu, O.H., Bhagwat, G., Oluyoye, I., Benson, N.U., Ayejuyo, O.O., Palanisami, T., 2020. Interaction of chemical contaminants with microplastics: principles and perspectives. Sci. Total Environ. 706, 135978.
González-Pleiter, M., Tamayo-Belda, M., Pulido-Reyes, G., Amariei, G., Leganés, F., Rosal, R., Fernández-Piñas, F., 2019. Secondary nanoplastics released from a biodegradable microplastic severely impact freshwater environments. Environ. Sci. -Nano 6 (5), 1382–1392.
Gullberg, E., Albrecht, L.M., Karlsson, C., Sandegren, L., Andersson, D.I., 2014. Selection of a multidrug resistance plasmid by sublethal levels of antibiotics and heavy metals. MBio 5 (5), e01918–14.
Guo, M.T., Yuan, Q.B., Yang, J., 2015. Distinguishing effects of ultraviolet exposure and chlorination on the horizontal transfer of antibiotic resistance genes in municipal wastewater. Environ. Sci. Technol. 49 (9), 5771–5778.
Han, X., Lv, P., Wang, L.-G., Long, F., Ma, X.-L., Liu, C., Feng, Y.-J., Yang, M.-F., Xiao, X., 2020. Impact of nano-$TiO_2$ on horizontal transfer of resistance genes mediated by filamentous phage transduction. Environ. Sci. -Nano 7 (4), 1214–1224.
He, Y., Yuan, Q., Mathieu, J., Stadler, L., Senehi, N., Sun, R., Alvarez, P.J.J., 2020. Antibiotic resistance genes from livestock waste: occurrence, dissemination, and treatment. npj Clean. Water 3 (1), 1–11.
Hebner, T.S., Maurer-Jones, M., 2020. Characterizing microplastic size and morphology of photodegraded polymers placed in simulated moving water conditions. Environ. Sci. -Proc. Imp. 22 (2), 398–407.
Hermansson, M., Linberg, C., 1994. Gene-transfer in the marine-environment. FEMS Microbiol. Ecol. 15 (1–2), 47–54.
Huang, Y.T., Yamauchi, Y., Lai, C.W., Chen, W.J., 2014. Evaluating the antibacterial property of gold-coated hydroxyapatite: a molecular biological approach. J. Hazard. Mater. 277, 20–26.
Huffer, T., Weniger, A.K., Hofmann, T., 2018. Sorption of organic compounds by aged polystyrene microplastic particles. Environ. Pollut. 236, 218–225.
Jiang, X., Ellabaan, M.M.H., Charusanti, P., Munck, C., Blin, K., Tong, Y., Weber, T., Sommer, M.O.A., Lee, S.Y., 2017. Dissemination of antibiotic resistance genes from antibiotic producers to pathogens. Nat. Commun. 2017 (8), 15784.
Jin, M., Liu, L., Wang, D., Yang, D., Liu, W., Yin, J., Yang, Z., Wang, H., Qiu, Z., Shen, Z., Shi, D., Li, H., Guo, J., Li, J., 2020. Chlorine disinfection promotes the exchange of antibiotic resistance genes across bacterial genera by natural transformation. ISME J. 14 (7), 1847–1856.
Jucker, B.A., Zehnder, A.J.B., Harms, H., 1998. Quantification of polymer interactions in bacterial adhesion. Environ. Sci. Technol. 32 (19), 2909–2915.
Karkman, A., Pärnänen, K., Larsson, D.G.J., 2019. Fecal pollution can explain antibiotic resistance gene abundances in anthropogenically impacted environments. Nat. Commun. 10 (1), 80.
Larrieu, J., Held, B., Martinez, H., Tison, Y., 2005. Ageing of atactic and isotactic polystyrene thin films treated by oxygen DC pulsed plasma. Surf. Coat. Technol. 200 (7), 2310–2316.
Lavonen, E., Kothawala, D., Tranvik, L., Köhler, S., 2014. Differential fluorescence EEMs can be used to assess treatability of DOM during drinking water production. EGUGA 12253.
Lee, Y.K., Murphy, K.R., Hur, J., 2020. Fluorescence signatures of dissolved organic matter leached from microplastics: polymers and additives. Environ. Sci. Technol. 54 (19), 11905–11914.
Lin, J., Yan, D., Fu, J., Chen, Y., Ou, H., 2020. Ultraviolet-C and vacuum ultraviolet inducing surface degradation of microplastics. Water Res. 186, 116360.
Liu, G., Zhu, Z., Yang, Y., Sun, Y., Yu, F., Ma, J., 2019a. Sorption behavior and mechanism of hydrophilic organic chemicals to virgin and aged microplastics in freshwater and seawater. Environ. Pollut. 246, 26–33.
Liu, H., Yang, D., Yang, H., Zhang, H., Zhang, W., Fang, Y., Lin, Z., Tian, L., Lin, B., Yan, J., Xi, Z., 2013. Comparative study of respiratory tract immune toxicity induced

by three sterilisation nanoparticles: silver, zinc oxide and titanium dioxide. J. Hazard. Mater. 248, 478–486.
Liu, X., Tang, J., Wang, L., Giesy, J.P., 2018. Mechanisms of oxidative stress caused by CuO nanoparticles to membranes of the bacterium Streptomyces coelicolor M145. Ecotox. Environ. Saf. 158, 123–130.
Mammo, F.K., Amoah, I.D., Gani, K.M., Pillay, L., Ratha, S.K., Bux, F., Kumari, S., 2020. Microplastics in the environment: interactions with microbes and chemical contaminants. Sci. Total Environ. 743, 140518.
Marchal, C., Perrin, D., Hedgpeth, J., Hofnung, M., 1980. Synthesis and maturation of lambda receptor in *Escherichia coli* K-12: *In vivo* and in vitro expression of gene *lamB* under *lac* promoter control. Proc. Natl. Acad. Sci. USA 77 (3), 1491–1495.
Mei, W., Chen, G., Bao, J., Song, M., Li, Y., Luo, C., 2020. Interactions between microplastics and organic compounds in aquatic environments: a mini review. Sci. Total Environ. 736, 139472.
Metcalf & Eddy, 2014. Wastewater Engineering: Treatment and Resource Recovery. 5th Edition, New York.
Miao, L., Gao, Y., Adyel, T.M., Huo, Z., Liu, Z., Wu, J., Hou, J., 2021. Effects of biofilm colonization on the sinking of microplastics in three freshwater environments. J. Hazard. Mater. 413, 125370.
Michielssen, S., Vedrin, M.C., Guikema, S.D., 2020. Trends in microbiological drinking water quality violations across the United States. Environ. Sci. -Water Res. 6 (11), 3091–3105.
Ochman, H., Lawrence, J.G., Groisman, E.A., 2000. Lateral gene transfer and the nature of bacterial innovation. Nature 405 (6784), 299–304.
Pazda, M., Kumirska, J., Stepnowski, P., Mulkiewicz, E., 2019. Antibiotic resistance genes identified in wastewater treatment plant systems–a review. Sci. Total Environ. 697, 134023.
Pham, D.N., Clark, L., Li, M., 2021. Microplastics as hubs enriching antibiotic-resistant bacteria and pathogens in municipal activated sludge. J. Hazard. Mater. Lett. 2, 100014.
Qiu, Z., Yu, Y., Chen, Z., Jin, M., Yang, D., Zhao, Z., Wang, J., Shen, Z., Wang, X., Qian, D., Huang, A., Zhang, B. and Li, J.W., 2012. Nanoalumina promotes the horizontal transfer of multiresistance genes mediated by plasmids across genera. Proc. Natl. Acad. Sci. U. S. A. 109 (13), 4944–4949.
Rochman, C.M., 2018. Microplastics research—from sink to source. Science 360 (6384), 28–29.
Selvam, S., Jesuraja, K., Venkatramanan, S., Roy, P.D., Kumari, V.J., 2021. Hazardous microplastic characteristics and its role as a vector of heavy metal in groundwater and surface water of coastal south India. J. Hazard. Mater. 402, 123786.
Song, Y.K., Hong, S.H., Jang, M., Han, G.M., Jung, S.W., Shim, W.J., 2017. Combined effects of uv exposure duration and mechanical abrasion on microplastic fragmentation by polymer type. Environ. Sci. Technol. 51 (8), 4368–4376.
Sun, D., Jeannot, K., Xiao, Y., Knapp, C.W., 2019a. Horizontal gene transfer mediated bacterial antibiotic resistance. Front. Microbiol. 10, 1933.
Sun, J., Dai, X., Wang, Q., van Loosdrecht, M.C.M., Ni, B.-J., 2019b. Microplastics in wastewater treatment plants: detection, occurrence and removal. Water Res 152, 21–37.
Tian, L., Chen, Q., Jiang, W., Wang, L., Xie, H., Kalogerakis, N., Ma, Y., Ji, R., 2019. A carbon-14 radiotracer-based study on the phototransformation of polystyrene nanoplastics in water versus in air. Environ. Sci. -Nano 6 (9), 2907–2917.
Vieira, J.C., Soares, L.C., Froes-Silva, R.E.S., 2018. Comparing chemometric and Langmuir isotherm for determination of maximum capacity adsorption of arsenic by a biosorbent. Microchem. J. 137, 324–328.
Wang, L., Yuan, L., Li, Z.H., Zhang, X., Sheng, G.P., 2021. Quantifying the occurrence and transformation potential of extracellular polymeric substances (EPS)-associated antibiotic resistance genes in activated sludge. J. Hazard. Mater. 408, 124428.
Wang, Q., Mao, D.Q., Luo, Y., 2015. Ionic liquid facilitates the conjugative transfer of antibiotic resistance genes mediated by plasmid RP4. Environ. Sci. Technol. 49 (14), 8731–8740.
Wang, W., Wang, J., 2018. Comparative evaluation of sorption kinetics and isotherms of pyrene onto microplastics. Chemosphere 193, 567–573.
Weinbauer, M.G., 2004. Ecology of prokaryotic viruses. FEMS Microbiol. Rev. 28 (2), 127–181.
von Wintersdorff, C.J.H., Penders, J., van Niekerk, J.M., Mills, N.D., Majumder, S., van Alphen, L.B., Savelkoul, P.H.M., Wolffs, P.F.G., 2016. Dissemination of antimicrobial resistance in microbial ecosystems through horizontal gene transfer. Front. Microbiol. 7, 173.
Xue, Y., Li, X., Li, H., Zhang, W., 2014. Quantifying thiol–gold interactions towards the efficient strength control. Nat. Commun. 5 (1), 1–9.
Yang, C., Sun, W., Ao, X., 2019. Using mRNA to investigate the effect of low-pressure ultraviolet disinfection on the viability of E. coli. Front. Env. Sci. Eng. 13 (2), 26.
Yang, Y., Shi, W., Lu, S.-Y., Liu, J., Liang, H., Yang, Y., Duan, G., Li, Y., Wang, H., Zhang, A., 2018. Prevalence of antibiotic resistance genes in bacteriophage DNA fraction from Funan River water in Sichuan, China. Sci. Total Environ. 626, 835–841.
Yu, Z., Wang, Y., Henderson, I.R., Guo, J., 2021. Artificial sweeteners stimulate horizontal transfer of extracellular antibiotic resistance genes through natural transformation. ISME J. 1–11.
Yuan, Q., Huang, Y., Wu, W., Zuo, P., Hu, N., Zhou, Y., Alvarez, P.J.J., 2019. Redistribution of intracellular and extracellular free & adsorbed antibiotic resistance genes through a wastewater treatment plant by an enhanced extracellular DNA extraction method with magnetic beads. Environ. Int. 131, 104986.
Yuan, Q., Zhang, D., Yu, P., Sun, R., Javed, H., Wu, G., Alvarez, P.J.J., 2020. Selective adsorption and photocatalytic degradation of extracellular antibiotic resistance genes by molecularly-imprinted graphitic carbon nitride. Environ. Sci. Technol. 54 (7), 4621–4630.
Zarei-Baygi, A., Smith, A.L., 2021. Intracellular versus extracellular antibiotic resistance genes in the environment: prevalence, horizontal transfer, and mitigation strategies. Bioresour. Technol. 319, 124181.
Zhang, B., Yu, P., Wang, Z., Alvarez, P.J.J., 2020a. Hormetic promotion of biofilm growth by polyvalent bacteriophages at low concentrations. Environ. Sci. Technol. 54 (19), 12358–12365.
Zhang, H., Wang, J., Zhou, B., Zhou, Y., Dai, Z., Zhou, Q., Chriestie, P., Luo, Y., 2018. Enhanced adsorption of oxytetracycline to weathered microplastic polystyrene: kinetics, isotherms and influencing factors. Environ. Pollut. 243, 1550–1557.
Zhang, S., Lu, J., Wang, Y., Verstraete, W., Yuan, Z., Guo, J., 2021a. Insights of metallic nanoparticles and ions in accelerating the bacterial uptake of antibiotic resistance genes. J. Hazard. Mater. 421, 126728.
Zhang, S., Wang, Y., Lu, J., Yu, Z., Song, H., Bond, P.L., Guo, J., 2021b. Chlorine disinfection facilitates natural transformation through ROS-mediated oxidative stress. ISME J. 15, 2969–2985.
Zhang, Y., Lu, J., Wu, J., Wang, J., Luo, Y., 2020b. Potential risks of microplastics combined with superbugs: enrichment of antibiotic resistant bacteria on the surface of microplastics in mariculture system. Ecotox. Environ. Saf. 187, 109852.